Development of Particle Morphology in Emulsion Polymerization. 1. Cluster Dynamics

Luis J. González-Ortiz[†] and José M. Asua*

Grupo de Ingeniería Química, Departamento de Química Aplicada, Facultad de Ciencias Químicas, Universidad del País Vasco, Apdo. 1072, 20080 San Sebastián, Spain

Received July 7, 1994; Revised Manuscript Received January 17, 1995[⊗]

ABSTRACT: A mathematical model for cluster migration during the development of the particle morphology in emulsion polymerization has been developed. The motion of the clusters is due to the balance between the van der Waals forces and the viscous forces. Several illustrative calculations are presented including systems for which the final equilibrium morphologies were (i) core–shell, (ii) inverted core–shell, and (iii) occluded morphology.

Introduction

Many practical benefits can be obtained by blending polymers. Thus, processability, chemical and environmental resistance, adhesion, and mechanical properties of polymer blends are superior to those of their homopolymers.[1] The performance of polymer blends depends heavily on their morphology.[2] Structured particles can be regarded as a special kind of polymer blend, for which the performance in a given application is determined by their morphology. Composite latex particles with a well-defined particle morphology are used to improve the mechanical properties of polymers,[3–5] to enhance adhesion properties[6] and to modify the latex viscosity by varying the degree of neutralization.[7] In addition, these particles are used in many other applications such as molecular carriers[8] and coatings.[9] Practical importance and scientific interest have been the driving force for much of the work published in recent years on latex particle morphology.[3–52]

The formation of a structured latex particle occurs through the following series–parallel processes:

(a) The polymer chains are formed at a given position in the polymer particle.

(b) If the newly formed polymer chain is incompatible with the polymer existing in the position where it is formed, phase separation occurs. Phase separation leads to the formation of clusters.

(c) In order to minimize the Gibbs free energy, the clusters migrate toward the equilibrium morphology. During this migration the size of the clusters may increase by (i) polymerization of monomer inside the cluster, (ii) diffusion of polymer chains into the cluster, and (iii) coagulation with other clusters. The rates of processes ii and iii depend strongly on the particle viscosity.

Several authors have reported theoretical approaches aimed at predicting the particle morphology. These approaches fall into two limiting situations: (i) The polymer chains do not move from the locus where they are formed (with the exception of the movement due to the increase of the particle volume).[10,12,26,30–32,52] (ii) The polymer chains are completely mobile and hence the equilibrium morphology is reached.[35,39,40,46,48,51]

The first limiting situation may occur when the newly formed polymer chains are compatible with the existing polymer as well as if the polymers are incompatible. Thus, Grancio and Williams[10] reported the formation of structured latex particles in the emulsion homopolymerization of styrene. For incompatible polymer systems, this limiting case may occur in the emulsion polymerization carried out under starved conditions in systems where the T_g of the polymer is higher than the reaction temperature. Two different models have been reported for this limiting case: (1) Models based on the repulsive wall effect[12,32,52] in which a monomer-rich shell develops due to the decrease in entropy of a polymer chain located near the surface of the particle and (2) models based on the anchoring of the hydrophilic end group of the growing polymer chain on the surface of the particle.[26,30,31]

The second limiting situation requires incompatible polymers and a low particle viscosity. Under these circumstances, there are no restrictions to either polymer chain diffusion or cluster migration and the equilibrium morphology is reached instantaneously. The models developed for this limiting case are based on thermodynamic considerations. In these models it is assumed that the total free energy change is equal to the interfacial energy change; i.e., no mixing and demixing effects are involved. Therefore, the thermodynamically preferred morphology is the one that has the minimum interfacial energy change. Based on the pioneering work of Torza and Mason,[53] calculations of the latex particle morphology that has the minimum interfacial energy change have been reported by Sundberg et al.[35] and Chen et al.[39,40] for some of the geometries considered by Torza and Mason.[53] Durant and Guillot[48] proposed a rather complex iterative algorithm to solve all the geometries considered by Torza and Mason.[53] Sundberg and Sundberg[51] studied the particle morphology for a system with more than three phases. In addition, Winzor and Sundberg[46] reported an equilibrium thermodynamic approach to predict the particle morphology as a function of the extent of conversion of a seeded emulsion polymerization. The basic assumption of this model is that, at any time, the polymer particle has the equilibrium morphology.

An extensive experimental program has been carried out by Chen et al.[39,40,44,45,47] to verify the predictions of the thermodynamic model. Comparisons between experimental results and model predictions have also been reported by Sundberg et al.[35,41] A good agreement

* To whom correspondence should be addressed.
[†] On leave from Universidad de Guadalajara, Guadalajara, México.
[⊗] Abstract published in *Advance ACS Abstracts,* April 1, 1995.

0024-9297/95/2228-3135$09.00/0

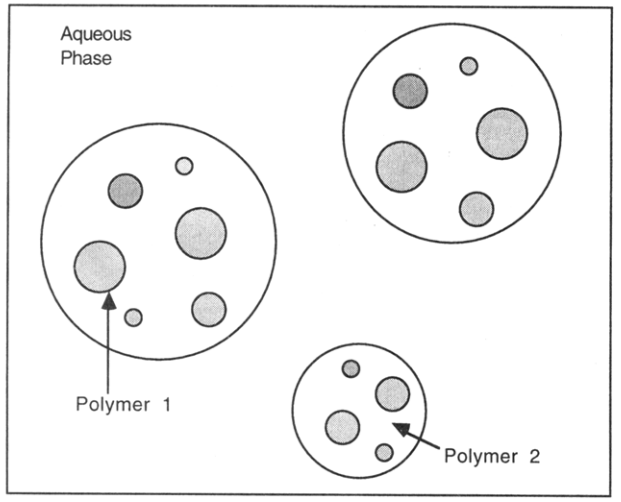

Figure 1. Nonreacting latex system.

between experimental results and model predictions was obtained for the cases in which the equilibrium morphology was reached. However, nonequilibrium morphologies were found when the viscosity of the polymer particles was high.[34,38] Similar results were reported by Jönsson et al.[37,64] These results show that kinetic factors such as the location in which the polymer is formed and the rates of both polymer diffusion and cluster migration can determine the morphology of the polymer particles. The development of a mathematical model including all the kinetic and thermodynamic factors is an obvious goal in the research of latex particle morphology. A way to achieve this goal is to first develop adequate models for each process and then to combine them in a global model. This is the approach chosen in the present investigation. In the first paper of this series a model for cluster migration is presented. Subsequent papers will include simultaneous polymerization and cluster migration and simultaneous polymerization, polymer chain diffusion, and cluster nucleation and migration.

Theory

The goal of the present paper is to develop a model for cluster migration; nucleation of the clusters and polymerization are beyond the scope of this work. Therefore, let us consider the nonreacting latex system made up of composite polymer particles such as those presented in Figure 1. These polymer particles contain clusters of polymer 1 dispersed in a matrix of polymer 2. The aqueous phase will be denoted as phase 3. It is assumed that both polymers 1 and 2 are at a temperature above their T_g. Therefore, the clusters of polymer 1 can move inside the matrix of polymer 2 if a sufficient driving force exists and the clusters can coagulate between them. Under these circumstances, the system depicted in Figure 1, which is in a metastable state,[35,39] will evolve toward the equilibrium morphology.

The system described above resembles the experiments reported by Jönsson et al.[37] These authors formed composite particles with morphologies similar to that presented in Figure 1 by polymerizing methyl methacrylate in the presence of polystyrene seed particles. Later, the equilibrium morphology was reached by reducing the viscosity of the system by treating the latexes with methylene chloride, a common solvent for both polystyrene and poly(methyl methacrylate). Some of the aging experiments reported by Min et al.,[19] in particular those with a low degree of grafting, also may be included in the system under consideration.

The dynamics of the clusters can be divided into two different parts: the motion of the clusters and the coagulation of the clusters. The motion of the clusters refers to situations in which the distance between the surfaces of two clusters is not negligible as compared with the cluster radius. In this case, the motion is due to the balance of two forces: (i) van der Waals attraction−repulsion forces and (ii) the resistance to flow that arises from viscous drag.

When the particles have contact, the interfacial tension forces[54−56] and the autohesion forces[57] promote the coalescence of spheres, which is hindered by the cluster resistance to deformation.[58]

A rough estimation of the time scale for the coagulation of clusters can be obtained from the Frenkel equation:[55]

$$t = \frac{2\pi r\mu}{3\theta^2\sigma_{ij}} \tag{1}$$

where r is the radius of the cluster, μ the viscosity of the cluster, θ the half-angle of coalescence, and σ_{ij} the interfacial tension. For $r = 10$ nm, $\mu = 10^8$ Pa s, and $\sigma_{ij} = 10$ dyn/cm, the time for complete coalescence ($\theta = \pi/2$) is about 100 s. It should be noted that the Frenkel equation underestimates the time for complete coagulation because viscous flow is considered to be the only resistance to particle deformation, whereas the contribution of the elastic deformation, which may be an important effect,[58] is neglected. Nevertheless, the time scale for the coagulation is generally much shorter than the time scale for the motion of the clusters (see below), and hence in the present model instantaneous coagulation of clusters is considered to occur once the surfaces of the clusters are closer than a critical arbitrary distance d_c.

The motion of the cluster j is controlled by the following equation:

$$m_j\frac{\mathrm{d}^2\mathbf{X}_j}{\mathrm{d}t^2} = \mathbf{F}_j - b_j\mu\frac{\mathrm{d}\mathbf{X}_j}{\mathrm{d}t} \tag{2}$$

where m_j is the mass of the cluster, $\mathbf{X}_j$ the vector giving the position of cluster j, $\mathbf{F}_j$ the net van der Waals force acting on the cluster, μ the viscosity of polymer 2, and b_j the friction factor that depends on the shape and size of the cluster ($b_j = 6\pi r_j$ for rigid spheres). $\mathbf{F}_j$ depends on the position of the cluster as well as on the positions of the other clusters and hence will change with time. Nevertheless, for an interval time in which the positions of the clusters do not change significantly, $\mathbf{F}_j$ can be considered to be constant. On the other hand, the movement of the clusters is very slow and, at the corresponding low shear rates, the viscosity of phase 2 is constant. For constant coefficients, eq 2 has the following analytical solution:

$$\mathbf{X}_j = \mathbf{X}_{j0} + \frac{\mathbf{F}_j}{b_j\mu}t + \frac{\mathbf{v}_0 m_j}{b_j\mu} - \frac{\mathbf{F}_j m_j}{(b_j\mu)^2} + \left[\frac{\mathbf{F}_j m_j}{(b_j\mu)^2} - \frac{\mathbf{v}_0 m_j}{b_j\mu}\right]\exp\left[-\frac{b_j\mu}{m_j}t\right] \tag{3}$$

where $\mathbf{X}_{j0}$ is the position of the cluster and $\mathbf{v}_0$ its velocity at $t = 0$. The assumption that μ = constant is not critical because the velocity of the clusters will be

extremely slow under most conditions for which the study of the particle morphology dynamics is worthwhile. On the other hand, the assumption that $\mathbf{F}_j$ is constant limits the use of eq 3 to small variation of the position of the clusters. It was found by simulation that $\mathbf{F}_j$ can be safely considered to be constant for movements $|\mathbf{X}_{j0} - \mathbf{X}_j| < 1$ nm.

Equation 3 can be further simplified taking into account the relative values of the different terms of the right-hand side member. For $r_j = 10$ nm, $\mu = 10^8$ Pa s, density of polymer 1 $\varrho_1 = 1100$ kg/m^3, and $t = 100$ s, the values of the different terms are

$$\frac{\mathbf{F}_j t}{b_j \mu} \cong 5.3\mathbf{F}_j \quad \text{(m)} \tag{4}$$

$$\frac{\mathbf{v}_0 m_j}{b_j \mu} \cong 2.4 \times 10^{-22}\mathbf{v}_0 \quad \text{(m)} \tag{5}$$

$$\frac{\mathbf{F}_j m_j}{(b_j \mu)^2} \cong 1.3 \times 10^{-23}\mathbf{F}_j \quad \text{(m)} \tag{6}$$

In addition, the ratio between $\mathbf{F}_j$ and $\mathbf{v}_0$ can be approximately estimated from the Stokes equation:

$$\frac{|\mathbf{F}_j|}{|\mathbf{v}_0|} = 6\pi r_j \mu \cong 19 \quad \text{(kg/s)} \tag{7}$$

Equations 4−7 show that without lack of accuracy eq 3 can be reduced to

$$\mathbf{X}_j = \mathbf{X}_{j0} + \frac{\mathbf{F}_j t}{b_j \mu} \tag{8}$$

Equation 8 is a simple algebraic equation that allows the accurate calculation of the motion of each cluster provided that small values of $|\mathbf{X}_{j0} - \mathbf{X}_j|$ are used. After each interval the net van der Waals force acting over each cluster has to be recalculated. This net force is given by

$$\mathbf{F}_j = \mathbf{F}_{j3} + \sum_{h=1,h\neq j}^{H} \mathbf{F}_{jh} \tag{9}$$

where H is the number of clusters, $\mathbf{F}_{jh}$ is the force over cluster j resulting from the interaction of clusters j and h, and $\mathbf{F}_{j3}$ is the force resulting from the interaction of cluster j and phase 3. These forces can be obtained from the energies of interaction, E_j, using the following equation:

$$\mathbf{F}_j = -\nabla E_j \tag{10}$$

The energy of interaction between two bodies depends on the shape and size of the bodies, their nature, and the nature of the phase between the bodies. In the system under consideration, several cases can arise. These cases are illustrated in Figure 2. This figure presents composite latex particles with clusters which are inside the latex particle as well as at the surface of the particle. The difference between Figures 2a and 2b lies in the shape of the clusters at the surface of the particles. The shape of each cluster is the shape that minimizes the interfacial energy around the cluster. In this work, the equilibrium morphologies are calculated as described in Appendix A. For the clusters inside the polymer particles, the minimum interfacial energy is

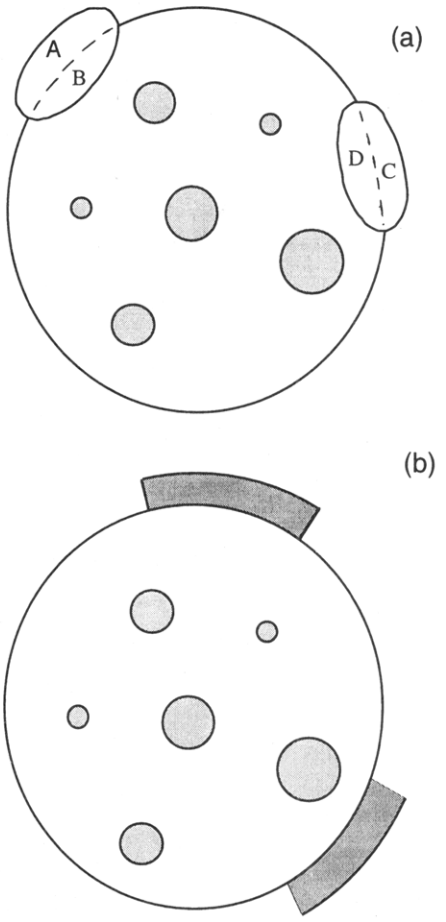

Figure 2. Composite latex particles.

provided by a spherical shape. However, when the cluster is on the surface, more complex situations can appear. In particular, Figure 2a presents the case in which the minimum interfacial energy corresponds to a cluster with an ellipsoidal shape, partially embedded in the polymer particle. On the other hand, in Figure 2b the equilibrium morphology of a cluster located at the surface of the particle is a continuous shell on the surface of the polymer particle. However, because this shell must have a minimum thickness, the amount of polymer 1 in each cluster can only form a patch on the surface of the polymer particle.

The following interactions occur in systems of composite latex particles such as those depicted in Figure 2.

(a) Attraction between two spherical particles of polymer 1 with radii r_1 and r_2 immersed in a continuous phase of polymer 2. The energy of interaction is[59,60]

$$E = -\frac{A_{121}}{6}\left\{\frac{2r_1r_2}{S^2-(r_1+r_2)^2} + \frac{2r_1r_2}{S^2-(r_1-r_2)^2} + \ln\left(\frac{S^2-(r_1+r_2)^2}{S^2-(r_1-r_2)^2}\right)\right\} \tag{11}$$

where A_{iji} is the Hamaker constant of material i in a continuous phase j and S the distance between the centers of the two spheres.

(b) Attraction−repulsion between an internal spherical cluster of polymer 1 and the aqueous phase. The energy of interaction is given by (see Appendix B)

$$E = -\frac{A_{123}}{3S_1}\left[\frac{r_1^3(R^2 - r_1^2 - 3S_1^2 - 2S_1R)}{[(R+S_1)^2 - r_1^2]^2} + \frac{r_1^3 + r_1S_1R - r_1S_1^2}{[(R-S_1)^2 - r_1^2]} - \frac{2r_1^3 + r_1S_1R + r_1S_1^2}{[(R+S_1)^2 - r_1^2]} - \frac{S_1}{2}\ln\left(\frac{R^2 - (S_1 - r_1)^2}{R^2 - (S_1 + r_1)^2}\right)\right] \quad (12)$$

with R the radius of the polymer particle and S_1 the radial position of the center of the cluster.

Notice that the value of A_{123} (see Appendix B) may be positive or negative, namely, attractive or repulsive. This will determine if the clusters will migrate toward the surface of the latex particle ($A_{123} > 0$) or toward the center of the particle ($A_{123} < 0$).

(c) Attraction between clusters partially embedded in the surface of the polymer particles. The energy of attraction between the two clusters of polymer 1 located at the surface of the polymer particle, such as in Figure 2a, is given by (see Appendix C)

$$E = A_{131}\Gamma_s(A,C) + A_{1(23)1}((\Gamma_s(A,D) + \Gamma_s(B,C)) + A_{121}\Gamma_s(B,D) \quad (13)$$

where A and C are the fractions of the clusters that are outside the polymer particle, B and D are the fractions of the clusters that are inside the polymer particle, and $\Gamma_s(I,J)$ are functions of the geometry and position of I and J. The calculation of $\Gamma_s(I,J)$ for all the possible geometries that can arise from the thermodynamic calculations would be intractable. Therefore, the respectives $\Gamma_s(I,J)$ were calculated considering that the fractions A, B, C, and D of the respective clusters were spheres, each fraction maintaining its corresponding volume. Equation 11 presents the geometry factor for spheres.

(d) Attraction between patch clusters on the surface of the polymer particles.

An analytical equation for the energy of attraction between two cylindrical clusters of radii r_1 and r_2 and height z is not available. However, solutions for limiting cases have been reported:[60]

$$E = -\left(\frac{r_1r_2}{r_1 + r_2}\right)^{1/2}\frac{A_{131}}{12\sqrt{2}S_2^{1.5}}z \qquad \text{for } r_1, r_2 \gg S_2 \quad (14)$$

$$E \approx -\frac{z}{S_2^5} \qquad \text{for } r_1, r_2 \ll S_2 \quad (15)$$

where S_2 is the distance between the surfaces of the cylinders. In this work, the energy of attraction is needed for the whole range of values of S_2. Therefore, the following approximate equation has been used:

$$E = -\left(\frac{r_1r_2}{r_1 + r_2}\right)^{1/2}\frac{A_{131}}{12\sqrt{2}S_2^{1.5}}z\left[\frac{1}{1 + \left(\frac{S_2}{r_1 + r_2}\right)^{3.5}}\right] \quad (16)$$

Illustrative Simulations

As explained in the Introduction, the goal of this work is to develop a model for cluster migration, the nucleation of the clusters and the polymerization being beyond the scope of the present paper. This is a burden for the illustrative simulations because an arbitrary initial state must be chosen and the evolution of the particle morphology is partially determined by the initial state. Therefore, the simulations detailed below cannot be claimed to be accurate descriptions of a real system because such a system includes processes other than cluster migration. Nevertheless, the simulations try to demonstrate in a semiquantitative way that the model is able to simulate the migration of the clusters properly.

Table 1. Values of the Main Parameters Used in the Illustrative Simulations

	equilibrium morphology		
	core–shell (case 1)	inverted core–shell (case 2)	occluded (case 3)
σ_{12} (dyn/cm)	4.0[a]	3.2[c]	1.63[d]
σ_{13} (dyn/cm)	19.5[b]	32.7[c]	5.66[d]
σ_{23} (dyn/cm)	35.0[b]	26.0[c]	4.46[d]
$A_{121} \times 10^{20}$ (J)[e]	0.78	0.63	0.32
$A_{131} \times 10^{20}$ (J)[e]	3.8		1.1
$A_{123} \times 10^{20}$ (J)[e]	1.9	−0.34	0.04
$A_{1(23)1} \times 10^{20}$ (J)[e]			0.28

[a] Wu.[65] [b] Hergeth et al.[63] [c] Jönsson et al.[37] [d] Chen et al.[47] [e] Estimated from the interfacial tensions as described in Appendix D.

The initial state for the simulations is a number of clusters (between 23 and 67 depending on the case) of polymer 1 dispersed in a latex particle of polymer 2 which in turn are dispersed in the aqueous phase (phase 3). These clusters have an arbitrary distribution of sizes and are randomly distributed in the latex particle. The shape of each cluster is the one that minimizes the interfacial energy around the cluster. For the clusters that are inside the latex particle, the minimum interfacial energy is provided by a spherical shape, but the shape of the clusters at the surface depends on the system under consideration. In this work, the equilibrium morphologies are calculated as detailed in Appendix A.

Simulations considering different particle morphologies under equilibrium conditions were carried out using the values of the parameters presented in Table 1. Note that the values of the interfacial tensions for apparently closely related systems are widely different. A possible explanation is the effect of the emulsifier used in each system. Nevertheless, in the simulation of each case we have tried to use the interfacial tensions from a single literature source. The Hamaker constants were estimated from the interfacial tensions as described in Appendix D. The illustrative simulations will be restricted to a single polymer particle that is assumed to represent the whole populations of polymer particles. In all the calculations, the volume fraction of the clusters was 0.30 and the viscosities of polymer 2 were selected, depending on the case, to be in the range from 10^5 to 10^8 Pa s.

Case 1 simulates a system for which the minimization of the total interfacial energy predicts a core–shell morphology under equilibrium conditions. For this simulation, the seed polymer was polystyrene and the second-stage polymer was poly(vinyl acetate). Figures 3–5 present the evolution of the particle morphology of case 1. These figures are the projections of the clusters on a vertical plane that rotates 180° about the vertical axis of the polymer particles. It can be seen that even in the initial state, the clusters in contact with the surface of the polymer particle form patches. This is the geometry of minimum interfacial energy considering a given minimum thickness (8 nm) of the polymer film. The internal clusters are spheres of different sizes.

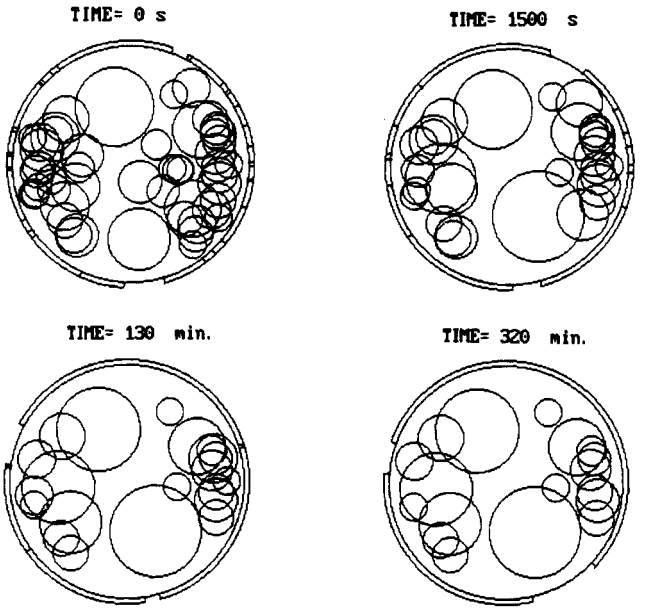

Figure 3. Initial stages in the evolution of the particle morphology for case 1 in Table 1. $\mu = 10^7$ Pa s.

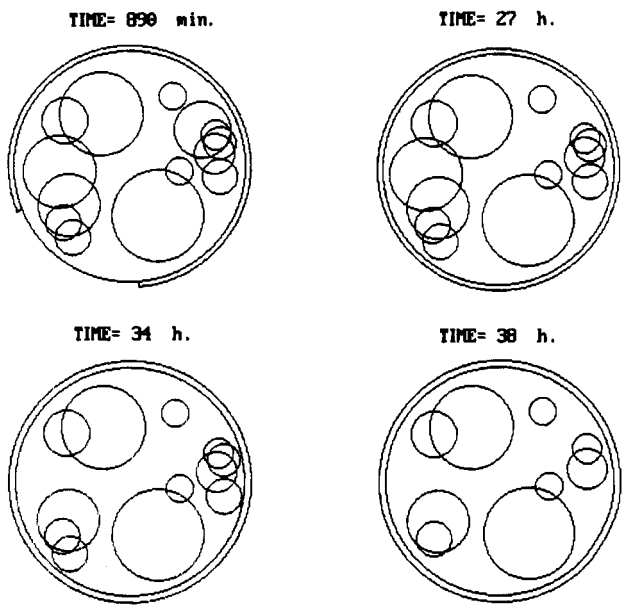

Figure 4. Middle stages in the evolution of the particle morphology for case 1 in Table 1. $\mu = 10^7$ Pa s.

Although Figure 3 suggests that there is a higher density of clusters near the surface of the particle than in the neighborhood of the center of the particle, this is an apparent artifact due to the type of projection used. Figures 3–5 show that clusters suffer mutual attraction leading to coagulation, and besides, they are attracted by the aqueous phase migrating toward the surface of the polymer particle. The size of the patches on the surface of the particle increases until eventually a continuous shell is formed. The time scale in which the whole process occurs mainly depends on the viscosity of polymer 2. Figures 6 and 7 present the evolution of the particle morphology for a lower viscosity of polymer 2. Comparison with Figures 3–5 shows that the development of the particle morphology is much quicker and the equilibrium morphology is reached in a shorter time.

Case 2 simulates a system for which an inverted core–shell is the equilibrium morphology. For this simulation, the seed polymer was poly(methyl methacrylate) and the second-stage polymer was polystyrene.

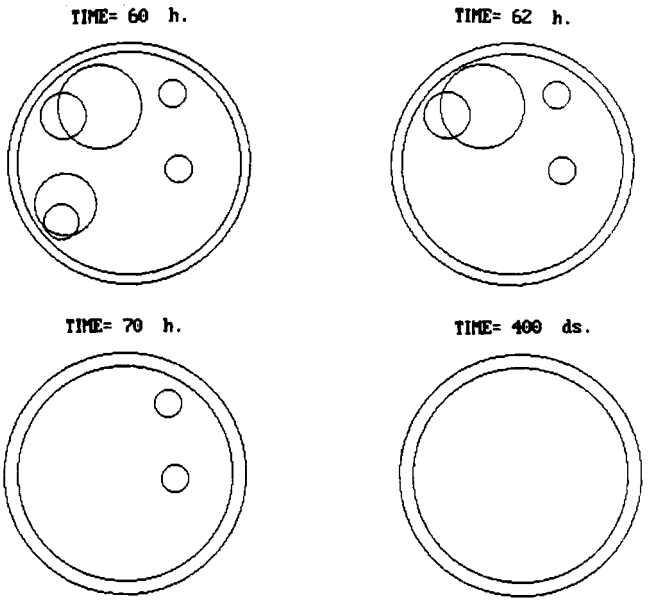

Figure 5. Final stages in the evolution of the particle morphology for case 1 in Table 1. $\mu = 10^7$ Pa s.

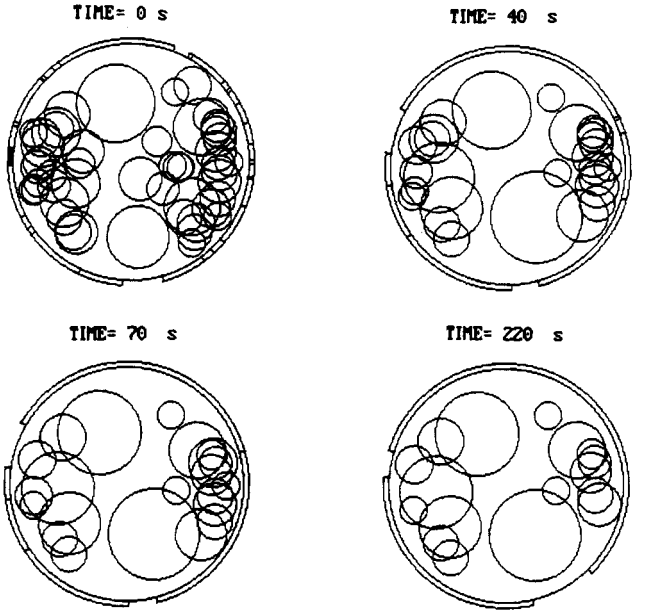

Figure 6. Initial stages in the evolution of the particle morphology for case 1 in Table 1. $\mu = 10^5$ Pa s.

Figures 8 and 9 present the evolution of the particle morphology for case 2 in Table 1. It can be seen that at the initial state, all the clusters, even those close to the particle surface, are inside the polymer particles because this is the morphology of minimum interfacial energy. The migration of the clusters is due to the fact that they attract each other leading to coagulation and are repelled by the aqueous phase toward the center of the particle. Jönsson et al.[64] studied the batch emulsion polymerization of styrene on a poly(methyl methacrylate) seed. The TEM micrographs of sectioned particles at the end of the polymerization showed clusters of polystyrene embedded in the poly(methyl methacrylate) particle with a low concentration of polystyrene cluster near the polymer surface. The micrographs resembled the particle morphologies presented in Figures 8 and 9 for intermediate times.

Case 3 simulates a system for which the minimization of the total interfacial energy predicts an occluded morphology. For this simulation, the seed polymer was

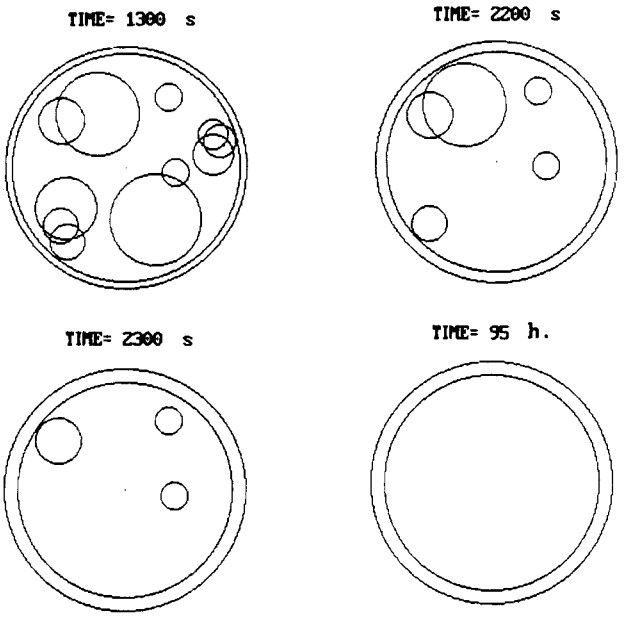

Figure 7. Final stages in the evolution of the particle morphology for case 1 in Table 1. $\mu = 10^5$ Pa s.

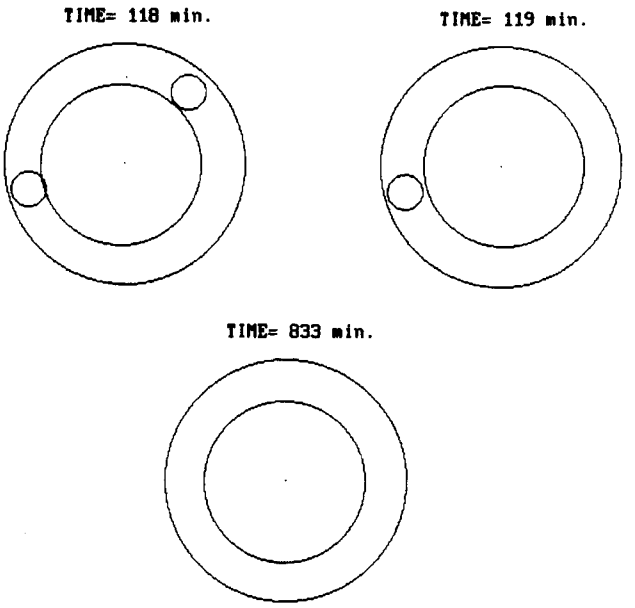

Figure 9. Final stages in the evolution of the particle morphology for case 2 in Table 1. $\mu = 10^8$ Pa s.

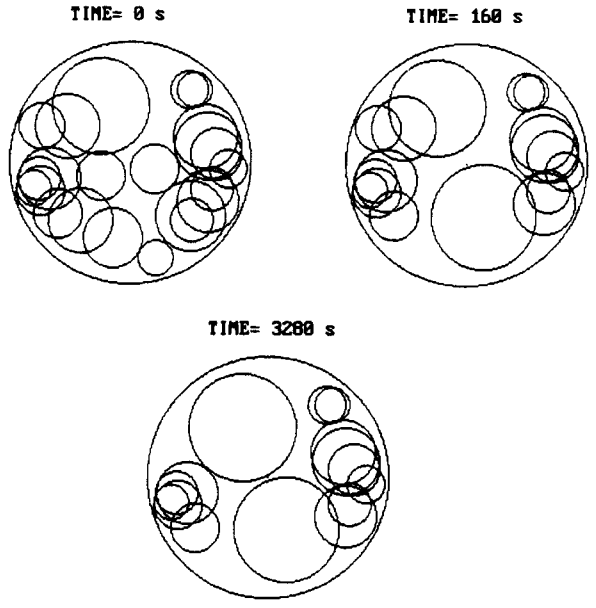

Figure 8. Initial stages in the evolution of the particle morphology for case 2 in Table 1. $\mu = 10^8$ Pa s.

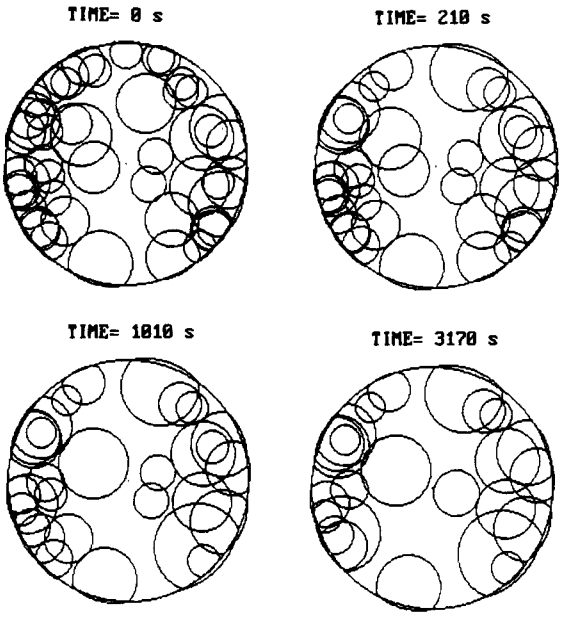

Figure 10. Initial stages in the evolution of the particle morphology for case 3 in Table 1. $\mu = 10^8$ Pa s.

polystyrene and the second-stage polymer was poly(methyl methacrylate). Chen et al.[47] studied this system polymerizing methyl methacrylate on the polystyrene seed and measured the interfacial tensions given in Table 1. Figures 10–12 present the evolution of the particle morphology. It can be seen that at the initial state, there are clusters embedded in the surface of the polymer particle and inside the polymer particle. The shape of the clusters at the surface of the particle is given by the minimization of the interfacial energy obtained using the values of the parameters given in Table 1 (case 3). Figures 10–12 show that in addition to the mutual coagulation of the clusters, they migrate toward the surface of the polymer particle where they also attract each other until the equilibrium morphology is reached. Unfortunately, the evolution of the particle morphology presented in Figures 10–12 cannot be checked against experimental results because Chen et al.[47] only reported micrographs of the equilibrium morphologies of the polymer particles. Nevertheless, the model gave the right trends and good agreement of the equilibrium morphologies was achieved. In addition, the predictions of the model showed similar trends to those found by Min et al.[19] in the aging of poly(butyl acrylate)/polystyrene composites particles with a low degree of grafting.

Conclusions

A mathematical model for cluster migration during the development of the latex particle morphology has been developed. A composite latex particle in which clusters of polymer 1 are dispersed in a matrix of polymer 2 is assumed to be the initial state. The motion of the clusters is due to the balance between the van der Waals forces and the viscous forces. The model includes the calculation of the forces of the interaction of one cluster with other clusters and with the aqueous phase. Several illustrative simulations were carried out

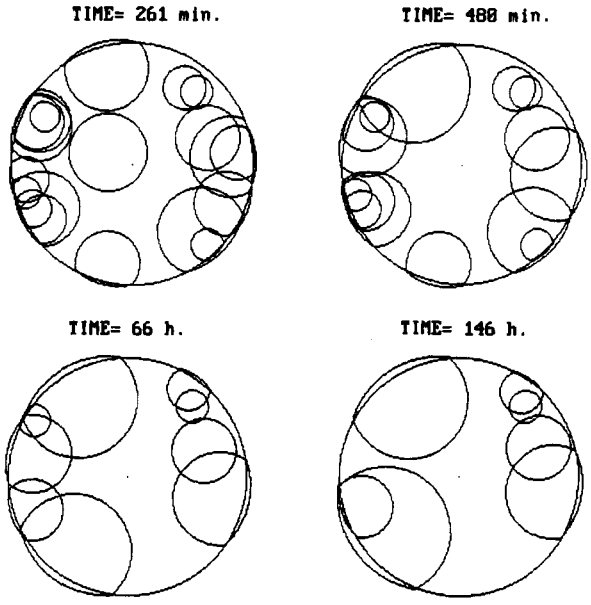

Figure 11. Middle stages in the evolution of the particle morphology for case 3 in Table 1. $\mu = 10^8$ Pa s.

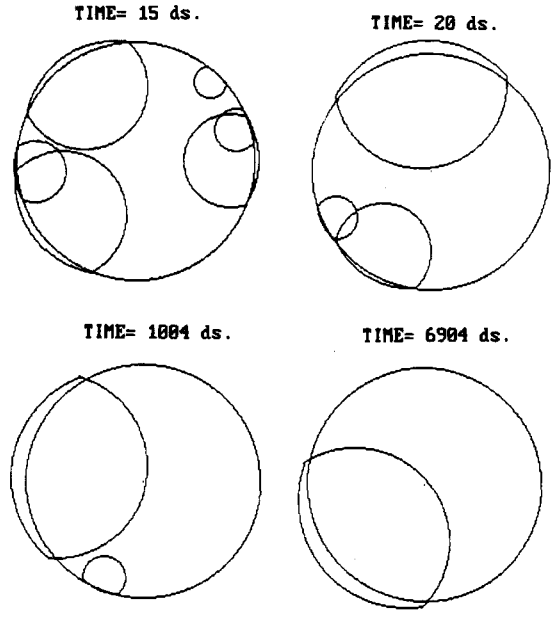

Figure 12. Final stages in the evolution of the particle morphology for case 3 in Table 1. $\mu = 10^8$ Pa s.

including systems for which the final equilibrium morphologies were (i) core–shell, (ii) inverted core–shell, and (iii) occluded morphology. The dynamics of the cluster migration depends heavily on the viscosity of the polymer matrix.

Acknowledgment. The AECI–UPV fellowship for L.J.G.-O. and the financial support by the Diputación Foral de Gipuzkoa are gratefully appreciated.

Nomenclature

a_{ij}	interfacial area between the phases i and j
A_{ik}	Hamaker constant for the interaction between the material i and the material k in vacuum
A_{ijk}	Hamaker constant for the interaction between the material i and the material k, both materials being immersed in a continuous phase j
b_j	friction factor of the cluster j
d_c	critical distance between the surfaces of the clusters at which instantaneous coagulation commences
E_j	energy of interaction of the cluster j
$\mathbf{F}_j$	net van der Waals force acting on cluster j
$\mathbf{F}_{jh}$	force acting on cluster j resulting from the interaction between clusters j and h
$\mathbf{F}_{j3}$	force acting on cluster j resulting from the interaction between cluster j and the phase 3
m_j	mass of the cluster j
r	radius of the cluster
R	radius of the polymer particle
R_{ij}	curvature radii of the interfacial area between the phases i and j
S	distance between the center of two interacting clusters
S_1	radial position of the center of the cluster with respect to the center of the particle
S_2	distance between the surfaces of two interacting cylinders
t	time
T	dimensionless interfacial tension defined by eq A-16
U	dimensionless interfacial tension defined by eq A-17
u_i	volume of polymer i
V_1	volume fraction of minority polymer
$\mathbf{v}_0$	initial velocity of the cluster j in each iterative step
$\mathbf{X}_j$	vector giving the position of the cluster j
$\mathbf{X}_{j0}$	initial position of the cluster j in each iterative step
z	height of each interacting cylinder

Greek Symbols

ϱ	density
ϕ	interfacial energy of the system
λ	London–van der Waals constant
$\Gamma_s(I,J)$	geometric factor for the energy of interaction between the bodies I and J
μ	viscosity
ϑ_{ij}	angle defined in Figure 13
σ_i	surface tension
σ_{ij}	interfacial tension
θ	half-angle of coalescence

Appendix A. Calculation of the Equilibrium Morphology

In the model it is assumed that the shape of each cluster is given by its equilibrium morphology. Clusters inside the polymer particles have a spherical shape but some calculations are needed to determine the equilibrium morphology when the clusters are at the surface of the particle. An additional interest to carry out this kind of calculation is to know which is the equilibrium morphology for the whole particle.

Following Torza and Mason,[53] let us consider volumes u_1 and u_2 of polymers 1 and 2, respectively, surrounded by a phase 3. The equilibrium morphology

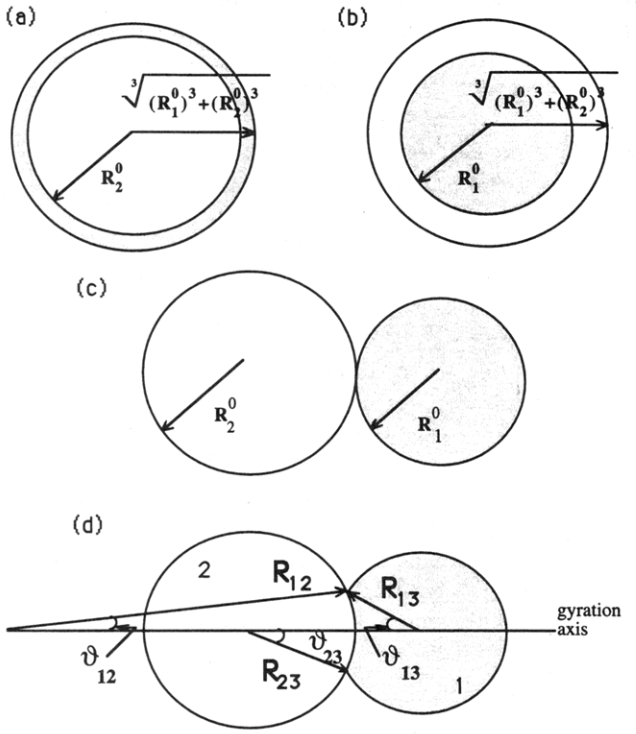

Figure 13. Geometries considered in the calculations of the thermodynamic equilibrium morphologies.

will be the one of those presented in Figure 13 that has the minimum interfacial energy,

$$\phi = \frac{1}{2}\sum_{i=1}^{3}\sum_{j=1,j\neq i}^{3} a_{ij}\sigma_{ij} \tag{A-1}$$

where a_{ij} and σ_{ij} are, respectively, the interfacial area and the interfacial tension between phases i and j.

The calculation of the interfacial energy for geometries a, b, and c in Figure 13 is straightforward but the calculation for case d is more complex because the actual shape of this morphology is not defined a priori but depends on the equilibrium morphology. Durand and Guillot[48] solved this case as an interfacial energy minimization problem, but this is a rather complex iterative procedure. Therefore, in this paper, the use of the equilibrium equations given by Torza and Mason[53] was preferred. These equations are as follows:

(i) Balance of capillary pressures across the interface 1−2 (Laplace equation):

$$\frac{\sigma_{13}}{R_{13}} = \frac{\sigma_{23}}{R_{23}} + \frac{\sigma_{12}}{R_{12}} \tag{A-2}$$

(ii) Balance of surface tension forces at the three-phase line:

$$\sigma_{12}\cos\vartheta_{12} = \sigma_{23}\cos\vartheta_{23} + \sigma_{13}\cos\vartheta_{13} \tag{A-3}$$

(iii) Geometric relationships:

$$R_{12}\sin\vartheta_{12} = R_{13}\sin\vartheta_{13} = R_{23}\sin\vartheta_{23} \tag{A-4}$$

(iv) Conservation of the volume of phase 1:

$$4(R_1^0)^3 = R_{13}^3[2 + \cos\vartheta_{13}(3 - \cos^2\vartheta_{13})] + R_{12}^3[2 - \cos\vartheta_{12}(3 - \cos^2\vartheta_{12})] \tag{A-5}$$

(v) Conservation of the volume of phase 2:

$$4(R_2^0)^3 = R_{23}^3[2 + \cos\vartheta_{23}(3 - \cos^2\vartheta_{23})] - R_{12}^3[2 - \cos\vartheta_{12}(3 - \cos^2\vartheta_{12})] \tag{A-6}$$

Combining eqs A-2 to A-6, the following implicit algebraic equation for ϑ_{23} is obtained:

$$\frac{(R_1^0)^3}{(R_2^0)^3} = \frac{\alpha_1 + \alpha_2}{\alpha_3 - \alpha_2} \tag{A-7}$$

where

$$\alpha_1 = \sin^3\vartheta_{23}\sin^3\vartheta_{12}(2 + \cos\vartheta_{13})(3 - \cos^2\vartheta_{13}) \tag{A-8}$$

$$\alpha_2 = \sin^3\vartheta_{23}\sin^3\vartheta_{13}(2 - \cos\vartheta_{12})(3 - \cos^2\vartheta_{12}) \tag{A-9}$$

$$\alpha_3 = \sin^3\vartheta_{12}\sin^3\vartheta_{13}(2 + \cos\vartheta_{23})(3 - \cos^2\vartheta_{23}) \tag{A-10}$$

$$\vartheta_{12} = \cos^{-1}\left[\frac{\sigma_{12}^2 + \sigma_{23}^2 - \sigma_{13}^2}{2\sigma_{23}\sigma_{12}}\right] - \vartheta_{23} = \alpha_4 - \vartheta_{23} \tag{A-11}$$

$$\vartheta_{13} = \tan^{-1}\left[\frac{\sigma_{23}\sin\vartheta_{23} + \sigma_{12}(\sin\alpha_4\cos\vartheta_{23} - \cos\alpha_4\sin\vartheta_{23})}{\sigma_{12}(\cos\alpha_4\cos\vartheta_{23} + \sin\alpha_4\sin\vartheta_{23}) - \sigma_{23}\cos\vartheta_{23}}\right] \tag{A-12}$$

Because more than one angle has the same value of the trigonometric functions and several trigonometric functions are involved in eqs A-7 to A-12, eq A-7 has multiple solutions for $0 < \vartheta_{23} < \pi$ but only one of them has physical meaning. The physical meaning of a particular solution can be easily checked by means of eqs A-2 to A-6. Therefore, a single-variable numerical method search was used to find the roots of eq A-7 and the value of ϑ_{23} that fulfills the original eqs A-2 to A-6 was chosen. ϑ_{12} and ϑ_{13} are given by eqs A-11 and A-12, and the curvature radii are as follows:

$$R_{23}^3 = 4(R_1^0)^3/\left[\left(\frac{\sin^3\vartheta_{23}}{\sin^3\vartheta_{13}}\right)(2 + \cos\vartheta_{13}(3 - \cos^2\vartheta_{13})) + \left(\frac{\sin^3\vartheta_{23}}{\sin^3\vartheta_{12}}\right)(2 - \cos\vartheta_{12}(3 - \cos^2\vartheta_{12}))\right] \tag{A-13}$$

$$R_{12} = R_{23}\frac{\sin\vartheta_{23}}{\sin\vartheta_{12}} \tag{A-14}$$

$$R_{13} = R_{23}\frac{\sin\vartheta_{23}}{\sin\vartheta_{13}} \tag{A-15}$$

Figures 14 and 15 present the results of these calculations as a function of the following parameters:

$$T = \frac{|\sigma_{13} - \sigma_{12}|}{\sigma_{23}} \tag{A-16}$$

$$U = \sigma_{12}/\sigma_{13} \tag{A-17}$$

$$V_1 = \frac{(R_1^0)^3}{[(R_1^0)^3 + (R_2^0)^3]} \tag{A-18}$$

where $|\sigma_{13} - \sigma_{12}|$ is the absolute value of $(\sigma_{13} - \sigma_{12})$.

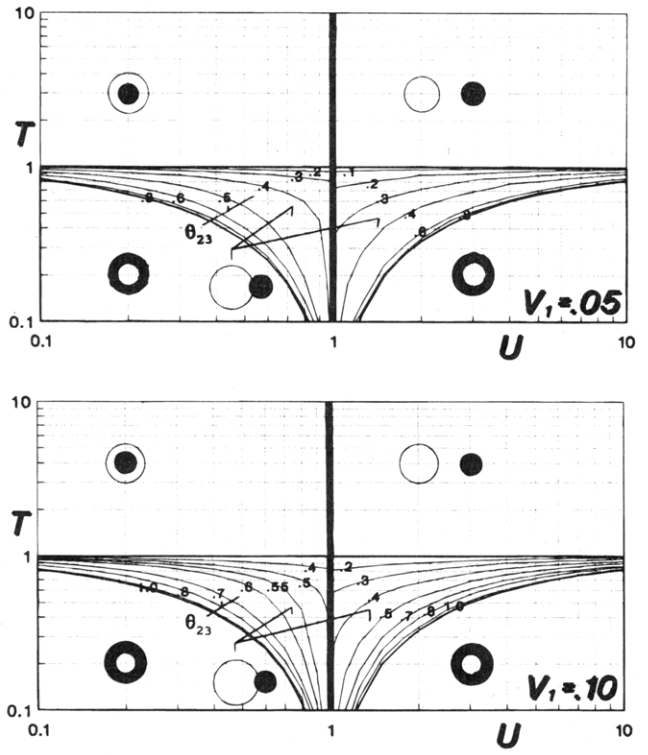

Figure 14. Equilibrium morphologies for $V_1 = 0.05$ and $V_1 = 0.10$.

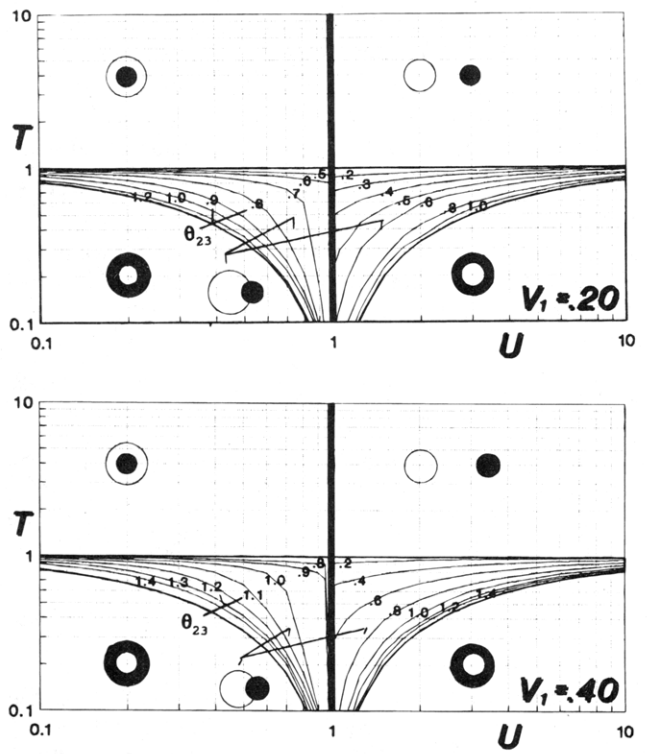

Figure 15. Equilibrium morphologies for $V_1 = 0.20$ and $V_1 = 0.40$.

Figures 14 and 15 show that individual particles will be obtained if $T > 1$ and $U > 1$; core–shell particles (core: majority polymer; shell: minority polymer) will be obtained if $T < |1 - U|/(1 + U)$; inverted core–shell particles (core: minority polymer; shell: majority polymer) will be obtained if $T > 1$ and $U < 1$; and an occluded morphology characterized by the value of ϑ_{23} given in the mentioned figures will be obtained otherwise.

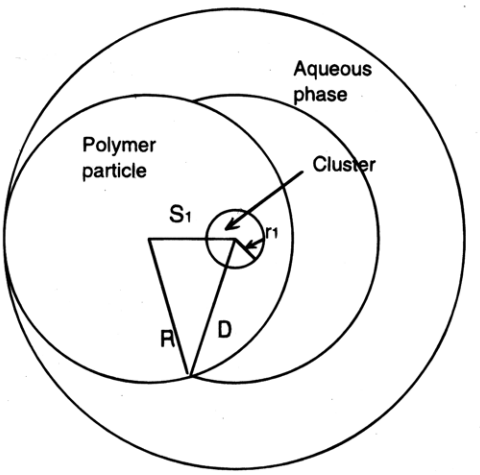

Figure 16. Interaction between an internal cluster and the aqueous phase.

Appendix B. Interaction between an Internal Cluster of Polymer 1 and the Aqueous Phase

The calculation of the total van der Waals interaction energy of an internal cluster of polymer 1 with the aqueous phase can be carried out following the approach developed by Hamaker.[61] The total interaction energy of a molecule of water with the internal spherical cluster is[61]

$$E_p = \frac{4\pi\lambda\varrho_1 r_1^3}{3(D^2 - r_1^2)^3} \tag{B-1}$$

where λ is the London–van der Waals constant, ϱ_1 the number of molecules per cm^3 of cluster, r_1 the diameter of the cluster, and D the distance between the center of the cluster and the molecule of water.

The total van der Waals interaction energy between the cluster and the aqueous phase is

$$E = -\varrho_3 \int_{\text{aqueous phase}} E_p \, dV \tag{B-2}$$

In order to calculate eq B-2, let us consider Figure 16. The total interaction energy between a cluster of radius r_1 located at a distance S_1 of the center of a polymer particle of radius R is determined by the interaction between the cluster with the molecules of water inside a sphere of radius $(S_1 + R)$ centered in the center of the cluster, because the effects of the water molecules outside this sphere will counteract one another due to the spherical symmetry. For the geometry presented in Figure 16, eq B-2 becomes

$$E = \varrho_3 \int_{R-S_1}^{R+S_1} E_p \left[\frac{\pi D}{S_1}((D + S_1)^2 - R^2)\right] dD \tag{B-3}$$

Substituting the value of E_p from eq B-1 into eq B-3 and integrating the resulting equation, the total interaction energy between an internal cluster and the aqueous phase is obtained:

$$E = -\frac{A_{13}}{3S_1}\left[\frac{r_1^3(R^2 - r_1^2 - 3S_1^2 - 2S_1R)}{[(R + S_1)^2 - r_1^2]^2} + \frac{r_1^3 + r_1S_1R - r_1S_1^2}{[(R - S_1)^2 - r_1^2]} - \frac{2r_1^3 + r_1S_1R + r_1S_1^2}{[(R + S_1)^2 - r_1^2]} - \frac{S_1}{2}\ln\left(\frac{R^2 - (S_1 - r_1)^2}{R^2 - (S_1 + r_1)^2}\right)\right] \tag{B-4}$$

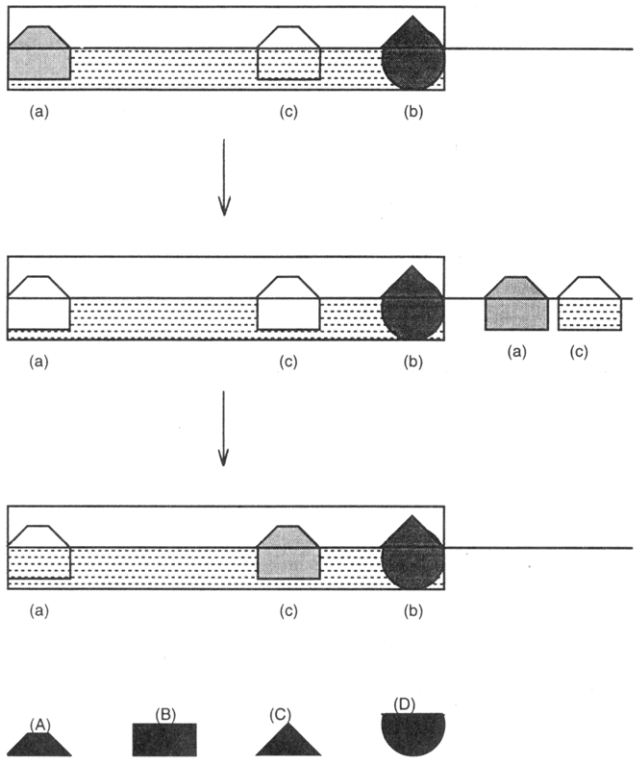

Figure 17. Thermodynamic path for calculating the interaction energy between clusters of polymer 1 at the surface of the polymer particle.

where the Hamaker constant is defined by

$$A_{13} = \pi^2 \varrho_1 \varrho_3 \lambda \tag{B-5}$$

Because the cluster and the aqueous phase are separed by polymer 2, A_{123}[60] should be used instead A_{13}.

$$A_{123} = A_{22} - A_{12} - A_{23} + A_{13} \tag{B-6}$$

Appendix C. Attraction between Clusters of Polymer 1 Located at the Surface of the Polymer Particles

To calculate the van der Waals interaction energy between clusters of polymer 1 located at the surface of the polymer particles, the approach described by Hunter[60] was used. The thermodynamic path presented in Figure 17 was considered. In the initial state the two clusters are infinitely separated (the shapes of the clusters are merely illustrative and by no means realistic). The molecules contained in the volume that will be finally occupied by cluster a can be considered as a cluster c.

If clusters a and c are removed from the medium leaving a vacuum, the change in free energy is

$$\Delta F = -F_1^{\mathrm{A}} - F_1^{\mathrm{B}} - (F_3^{\mathrm{A}} - V_{33}^{\mathrm{AC}}(s) + V_{31}^{\mathrm{AC}}(s) - V_{32}^{\mathrm{AD}}(s) + V_{31}^{\mathrm{AD}}(s)) - (F_2^{\mathrm{B}} - V_{22}^{\mathrm{BD}}(s) + V_{21}^{\mathrm{BD}}(s) - V_{23}^{\mathrm{BC}}(s) - V_{21}^{\mathrm{BC}}(s)) \tag{C-1}$$

where s is the distance between clusters b and c and F_i^{J} is the interaction energy of the isolated part J made of material i with the semiinfinite media 2 and 3. The energy change in removing cluster c includes the effect of the proximity of cluster b. Thus, the energy $V_{31}^{\mathrm{AC}}(s) - V_{33}^{\mathrm{AC}}(s) + V_{31}^{\mathrm{AD}}(s) - V_{32}^{\mathrm{AD}}(s)$ represents the change in the interaction energy of fraction A of cluster c with its environment when the molecules of polymer 2 and water that would have occupied the position of cluster b are replaced by cluster b.

The next step is to put cluster c into the hole occupied originally by cluster a and vice versa. The energy change is

$$\Delta F' = F_1^{\mathrm{A}} - V_{13}^{\mathrm{AC}}(s) + V_{11}^{\mathrm{AC}}(s) - V_{12}^{\mathrm{AD}}(s) + V_{11}^{\mathrm{AD}}(s) + F_1^{\mathrm{B}} - V_{13}^{\mathrm{BC}}(s) + V_{11}^{\mathrm{BC}}(s) - V_{12}^{\mathrm{BD}}(s) + V_{11}^{\mathrm{BD}}(s) + F_3^{\mathrm{A}} + F_2^{\mathrm{B}} \tag{C-2}$$

The interaction energy of clusters a and b at separation s at the surface is $E = \Delta F + \Delta F'$. In addition[60]

$$V_{ij}^{kh}(s) = A_{ij}\Gamma_s(k,h) \tag{C-3}$$

where A_{ij} is the vacuum Hamaker constant (for the materials i and j) and $\Gamma_s(k,h)$ is a positive function that depends only on the geometry of the system and is independent of the composition of the clusters a and b.

Combination of eqs C-1, C-2, and C-3 gives

$$E = (A_{33} - 2A_{13} + A_{11})\Gamma_s(A,C) + (A_{23} - A_{12} - A_{13} + A_{11})(\Gamma_s(A,D) + \Gamma_s(B,C)) + (A_{22} - 2A_{12} + A_{11})\Gamma_s(B,D) \tag{C-4}$$

Equation C-4 may be written as follows:

$$E = A_{131}\Gamma_s(A,C) + A_{1(23)1}((\Gamma_s(A,D) + \Gamma_s(B,C)) + A_{121}\Gamma_s(B,D) \tag{C-5}$$

Appendix D. Relationships between the Hamaker Constants and the Interfacial Tensions

The interfacial tensions between phases i and j is[60]

$$\sigma_{ij} = \sigma_i + \sigma_j + E_{ij} \tag{D-1}$$

where E_{ij} represents the work of adhesion between the two phases. E_{ij} is the van der Waals energy of interaction per unit area of interface given by

$$E_{ij} = \frac{-A_{ij}}{12\pi(L_c)_{ij}^2} \tag{D-2}$$

where A_{ij} is the Hamaker constant and $(L_c)_{ij}$ the "distance" between the phases.

On the other hand, the surface tension can be calculated by means of the following equation:[60]

$$\sigma_i = 0.5\frac{A_{ii}}{12\pi(L_c)_{ii}^2} \tag{D-3}$$

Equations D-1 to D-3 can be used to calculate the Hamaker constants needed in the model developed in this work in terms of the interfacial tensions. Thus

$$A_{123} = A_{22} - A_{12} - A_{23} + A_{13} \tag{D-4}$$

Combination of eqs D-1 to D-4 gives

$$A_{123} = 12\pi[(L_c)_{12}^2\sigma_{12} + (L_c)_{23}^2\sigma_{23} - (L_c)_{13}^2\sigma_{13} + \sigma_1((L_c)_{13}^2 - (L_c)_{12}^2)] + \sigma_2(2(L_c)_{22}^2 - (L_c)_{12}^2 - (L_c)_{23}^2) + \sigma_3((L_c)_{13}^2 - (L_c)_{23}^2)] \tag{D-5}$$

L_c is inversely proportional to the square root of the density of the phases, and hence small variations

between the different L_c are expected.[60] This means that difference terms in eq D-5 can be safely neglected. Thus

$$A_{123} = 12\pi[(L_c)_{12}{}^2\sigma_{12} + (L_c)_{23}{}^2\sigma_{23} - (L_c)_{13}{}^2\sigma_{13}] \quad \text{(D-6)}$$

Similarly

$$A_{121} = A_{11} + A_{22} - 2A_{12} = 24\pi(L_c)_{12}{}^2\sigma_{12} \quad \text{(D-7)}$$

$$A_{131} = A_{11} + A_{33} - 2A_{13} = 24\pi(L_c)_{13}{}^2\sigma_{13} \quad \text{(D-8)}$$

$$A_{1(2,3)1} = A_{11} - A_{13} - A_{12} + A_{23} = 12\pi[(L_c)_{13}{}^2\sigma_{13} + (L_c)_{12}{}^2\sigma_{12} - (L_c)_{23}{}^2\sigma_{23}] \quad \text{(D-9)}$$

In the simulations presented in this work, it was considered that $(L_c)_{12}{}^2 = (L_c)_{13}{}^2 = (L_c)_{23}{}^2 = 2.6 \times 10^{-20}$ m^2 (value for decane given by Hough and White[62]).

References and Notes

(1) Deanin, R. D. In *Advances in Polymer Blends and Alloys Technology*; Technomic Publishing Co. Inc.: Lancaster, 1992; Vol. 3, Chapter 1.
(2) Deanin, R. D.; Deanin, A. A.; Sjoblom, T. In *Polymer Science and Technology*; Plenum Press: New York, 1974; Vol. 4, Chapter 2.
(3) Merkel, M. P.; Dimonie, V. L.; El-Aasser, M. S.; Vanderhoff, J. W. *J. Polym. Sci., Part A: Polym. Chem.* **1987**, *25*, 1219.
(4) Cook, D. G.; Rudin, A.; Plumtree, A. *J. Appl. Polym. Sci.* **1992**, *46*, 1387.
(5) Lovell, P. A.; McDonald, J.; Saunders, D. E. J.; Young, R. J. *Polymer* **1993**, *34*, 61.
(6) Sumi, H.; Takemura, A.; Kajiyama, M.; Hatano, Y.; Tomita, B.; Mizumachi, H. *J. Adhes.* **1992**, *38*, 173.
(7) Nishida, S.; El-Aasser, M. S.; Klein, A.; Vanderhoff, J. W. In *Emulsion Polymers and Emulsion Polymerization*; ACS Symp. Ser. 165; Basset, D. R., Hamielec, A. E., Eds.; American Chemical Society: Washington, DC, 1982; pp 290–314.
(8) Nustad, K.; Johansen, L.; Ugelstad, J.; Ellingsen, T.; Berge, A. *Eur. Sur. Res.* **1984**, *16*, Suppl. 2, 80.
(9) Vandezande, G.; Rudin, A. *J. Coat. Technol.* **1994**, *66*, 99.
(10) Grancio, M. R.; Williams, D. J. *J. Polym. Sci., Part A-1* **1970**, *8*, 2617.
(11) Keusch, P.; Prince, J.; Williams, D. J. *J. Macromol. Sci., Chem.* **1973**, *A7 (3)*, 623.
(12) Keusch, P.; Graff, R. A.; Williams, D. J. *Macromolecules* **1974**, *7*, 304.
(13) Okubo, M.; Katsuta, Y.; Matsumoto, T. *J. Polym. Sci., Polym. Lett. Ed.* **1980**, *18*, 481.
(14) Okubo, M.; Ando, M.; Yamada, A.; Katsuta, Y.; Matsumoto, T. *J. Polym. Sci., Polym. Lett. Ed.* **1981**, *19*, 143.
(15) Morgan, L. W. *J. Appl. Polym. Sci.* **1982**, *27*, 2033.
(16) Okubo, M.; Katsuta, Y.; Matsumoto, T. *J. Polym. Sci., Polym. Lett. Ed.* **1982**, *20*, 45.
(17) Okubo, M.; Sieke, M.; Matsumoto, T. *J. Appl. Polym. Sci.* **1983**, *28*, 383.
(18) Lee, D. I.; Ishikawa, T. *J. Polym. Sci., Polym. Chem. Ed.* **1983**, *21*, 147.
(19) Min, T. I.; Klein, A.; El-Aasser, M. S.; Vanderhoff, J. W. *J. Polym. Sci., Polym. Chem. Ed.* **1983**, *21*, 2845.
(20) Muroi, S.; Hashimoto, H.; Hosoi, K. *J. Polym. Sci., Polym. Chem. Ed.* **1984**, *22*, 1365.
(21) Dimonie, V.; El-Aasser, M. S.; Klein, A.; Vanderhoff, J. W. *J. Polym. Sci., Polym. Chem. Ed.* **1984**, *22*, 2197.
(22) Stutman, D. R.; Klein, A.; El-Aasser, M. S.; Vanderhoff, J. W. *Ind. Eng. Chem. Prod. Res. Dev.* **1985**, *24*, 404.
(23) Daniel, J. C. *Makromol. Chem. Suppl.* **1985**, *10/11*, 359.
(24) Zosel, A.; Heckmann, W.; Ley, G.; Mächtle, W. *Colloid Polym. Sci.* **1987**, *265*, 113.
(25) Kong, X. Z.; Pichot, C.; Guillot, J. *Colloid Polym. Sci.* **1987**, *265*, 791.
(26) Chern, C.-S.; Poehlein, G. W. *J. Polym. Sci., Part A: Polym. Chem.* **1987**, *25*, 617.
(27) Berg, J.; Sundberg, D.; Kronberg, B. *J. Microencapsulation* **1989**, *6*, 327.
(28) Hergeth, W.-D.; Bittrich, H.; Eichhorn, F.; Schlenker, S.; Schmutzler, K.; Steinan, U. J. *Polymer* **1989**, *60*, 1913.
(29) Lee, S.; Rudin, A. *Makromol. Chem., Rapid Commun.* **1989**, *10*, 655.
(30) de la Cal, J. C.; Urzay, R.; Zamora, A.; Forcada, J.; Asua, J. M. *J. Polym. Sci., Part A: Polym. Chem.* **1990**, *28*, 1011.
(31) Mills, M. F.; Gilbert, R. G.; Napper, D. H. *Macromolecules* **1990**, *23*, 4247.
(32) Yang, S. I.; Klein, A.; Sperling, L. H.; Cassasa, E. F. *Macromolecules* **1990**, *23*, 4582.
(33) Disanayaka, B.; Zhao, C. L.; Winnik, M. A.; Shivers, R.; Croucher, M. D. *Langmuir* **1990**, *6*, 162.
(34) Daniels, E. S.; Dimonie, V. L.; El-Aasser, M. S.; Vanderhoff, J. W. *J. Appl. Polym. Sci.* **1990**, *41*, 2463.
(35) Sundberg, D. C.; Casassa, A. P.; Pantazopoulos, J.; Muscato, M. R.; Kronberg, B.; Berg, J. *J. Appl. Polym. Sci.* **1990**, *41*, 1425.
(36) Okubo, M.; He, Y.; Ichikawa, K. *Colloid Polym. Sci.* **1991**, *269*, 125.
(37) Jönsson, J.-E. L.; Hassander, H.; Jansson, L. H.; Törnell, B. *Macromolecules* **1991**, *24*, 126.
(38) Rios, L.; Hidalgo, M.; Cavaille, J. Y.; Guillot, J.; Guyot, A.; Pichot, C. *Colloid Polym. Sci.* **1991**, *269*, 812.
(39) Chen, Y. C.; Dimonie, V. L.; El-Aasser, M. S. *J. Appl. Polym. Sci.* **1991**, *42*, 1049.
(40) Chen, Y. C.; Dimonie, V. L.; El-Aasser, M. S. *Macromolecules* **1991**, *24*, 3779.
(41) Muscato, M. R.; Sundberg, D. C. *J. Polym. Sci., Part B: Polym. Phys.* **1991**, *29*, 1021.
(42) Hidalgo, M.; Cavaille, J. Y.; Guillot, J.; Guyot, A.; Pichot, C.; Rios, L.; Vassoille, R. *Colloid Polym. Sci.* **1992**, *270*, 1208.
(43) Schellenberg, J.; Hamann, B. *Polymer* **1992**, *33*, 2802.
(44) Chen, Y. C.; Dimonie, V. L.; El-Aasser, M. S. *J. Appl. Polym. Sci.* **1992**, *45*, 487.
(45) Chen, Y. C.; Dimonie, V. L.; El-Aasser, M. S. *Pure Appl. Chem.* **1992**, *64(11)*, 1691.
(46) Winzor, C. L.; Sundberg, D. C. *Polymer* **1992**, *33*, 3797.
(47) Chen, Y. C.; Dimonie, V. L.; Shaffer, O. L.; El-Aasser, M. S. *Polym. Int.* **1993**, *30*, 185.
(48) Durant, Y. G. J.; Guillot, J. *Colloid Polym. Sci.* **1993**, *271*, 607.
(49) Kim, K. R.; An, J. H.; Cho, K. W.; Park, C. E. *J. Appl. Polym. Sci.* **1993**, *47*, 305.
(50) Cook, D. G.; Rudin, A.; Plumtree, A. *J. Appl. Polym. Sci.* **1993**, *48*, 75.
(51) Sundberg, E. J.; Sundberg, D. C. *J. Appl. Polym. Sci.* **1993**, *47*, 1277.
(52) Croxon, C. A.; Mills, M. F.; Gilbert, R. G.; Napper, D. H. *Macromolecules* **1993**, *26*, 3563.
(53) Torza, S.; Mason, S. G. *J. Colloid Interface Sci.* **1970**, *33(1)*, 67.
(54) Brown, G. L. *J. Polym. Sci.* **1956**, *22*, 423.
(55) Dillon, R. E.; Matheson, L. A.; Bradfors, E. B. *J. Colloid Sci.* **1951**, *6*, 108.
(56) Vanderhoff, J. W.; Tarkowsky, H. L.; Jenkins, M. C.; Bradford, E. B. *J. Macromol. Chem.* **1966**, *1*, 361.
(57) Voyutskii, S. S. *J. Polym. Sci.* **1958**, *32*, 528.
(58) Rios, L. *Makromol. Chem., Macromol. Symp.* **1990**, *35/36*, 389.
(59) Hiemenz, P. C. *Principles of Colloid and Surface Chemistry*; Marcel Dekker: New York, 1986.
(60) Hunter, R. J. *Foundations of Colloid Science*; Clarendon Press: Oxford, 1987; Chapters 4, 5.
(61) Hamaker, H. C. *Physica* **1937**, *4*, 1058.
(62) Hough, D. B.; White, L. R. *Adv. Colloid Interface Sci.* **1980**, *14*, 3.
(63) Hergeth, W. D.; Steinau, V. J.; Bittrich, H.; Schmutzler, K.; Wartewig, S. *Prog. Colloid Polym. Sci.* **1991**, *85*, 82.
(64) Jönsson, J.-E. L.; Hassander, H.; Törnell, B. *Macromolecules* **1994**, *27*, 1932.
(65) Wu, S. *Polymer Interface and Adhesion*; Marcel Dekker: New York, 1982; Chapter 3.

MA946102P